Electronic supplementary information (ESI) for

Atomically thin iridium nanosheets for oxygen evolution electrocatalysis

Hyeongbin Jo,‡[a] Younghyun Wy,‡[a] Hojin Ahn,[a] Yonghyeon Kim,[a] Bon Seung Goo,[a] Yongmin Kwon,[a] Jin Hong Kim,[b] Jin Sik Choi,[b] and Sang Woo Han*[a]

[a]Center for Nanotectonics, Department of Chemistry and KI for the NanoCentury, KAIST, Daejeon 34141, Korea. E-mail: sangwoohan@kaist.ac.kr
[b]Department of Physics, Konkuk University, Seoul 05029, Korea

‡ These authors contributed equally to this work.

Contents

1. Experimental details

Materials. $IrCl_4$ (99.95%), $IrBr_4$ (99.99%), IrI_4 (99.95%), and Ir black (99.95%) were purchased from Thermo Fisher Scientific. Di-*n*-octylamine and oleylamine were purchased from Acros Organics and TCI Chemicals, respectively. Trioctylamine, hydrochloric acid (37%, ACS reagent), *n*-butyllithium solution (2.5 M in hexane), Nafion solution (5 wt % in aliphatic alcohols and water), and 3 Å molecular sieves were purchased from Sigma−Aldrich. Ethyl alcohol and cyclohexane were provided by Daejung chemicals. Tetrahydrofuran and sulfuric acid were purchased from Junsei Chemical Co., Ltd. All the materials were used as received without further purification. Highly purified deionized water with a resistivity of 18.2 MΩ·cm was used in the preparation of aqueous solutions.

Preparation of Ir nanosheets. Ir nanosheets were synthesized by a solvothermal method. In a typical preparation of Ir nanosheets, 0.0334 g of $IrCl_4$ was mixed with 10 mL of di-*n*-octylamine solvent, which was dehydrated by heat-activated 3 Å molecular sieves before use, in a 100 mL rounded-bottom flask. After stirring the mixture for 10 min, 1.2 mL of *n*-butyllithium solution was added to the mixture. The resultant mixture was then heated to 290 °C with a ramping rate of 10 °C min^{-1} and kept at that temperature for 4 h under a CO flow condition (35 mL min^{-1}). Then, the mixture was cooled to room temperature and centrifuged to obtain the product. The prepared Ir nanosheets were washed several times with ethyl alcohol, hydrochloric acid-added tetrahydrofuran, and cyclohexane, and then dispersed in cyclohexane.

Characterizations. A FEI Tecnai F30 Super-Twin transmission electron microscope operated at 300 kV was used to obtain TEM images. HAADF–STEM images were obtained by a FEI Talos F2000X field-emission transmission electron microscope operated at 200 kV. TEM samples were prepared by dropping the colloidal suspension of Ir nanosheets onto a carbon-coated Cu grid (300 mesh). The XPS measurements were performed using a Thermo VG Scientific Sigma Probe spectrometer with an Al Kα X-ray source (1486.6 eV). To obtain XRD patterns, an RIGAKU Ultima IV thin-film X-ray diffractometer was used. AFM measurements were performed with a Seiko SPA-300HV atomic force microscope using a high-resolution cantilever with a diamondlike carbon (DLC) tip (NSG01 DLC, NT-MDT, Russia) with the tapping mode. To prepare AFM samples, a colloidal suspension of Ir nanosheets was spin-coated on a Si wafer and heat-treated at 600 °C for 20 h to remove organic adsorbates. An Agilent ICP-OES 5110 was used for the elemental analysis.

Electrochemical experiments. To prepare Ir nanosheet catalysts, 1 mg of Ir nanosheets were collected with centrifugation (10000 rpm for 15 min) and dispersed in 5 mL of ethanol. This nanosheet solution was mixed with 5 mL of ethanol containing Vulcan XC-72R (0.2 mg mL^{-1}) and sonicated for 2 h. The prepared Ir nanosheet catalysts were collected by centrifugation (13000 rpm for 10 min) and washed with ethanol and then dispersed in a solution containing 980 μL of ethanol, 980 μL of water, and 40 μL of a Nafion solution. The resultant mixture was sonicated for 2 h to form a homogeneous catalyst ink. The ICP–OES-determined Ir content of the catalyst ink was about 43.5 wt %. 20 μL of the catalyst ink was loaded on a rotating disk

electrode (RDE) with a diameter of 5 mm and dried at room temperature. An Ir black catalyst ink was prepared with the same method. Electrochemical experiments were conducted with a potentiostat (CH Instruments model 660E) in a three-electrode cell system consisting of an Ag/AgCl (in saturated KCl) reference electrode, a Pt wire as a counter electrode, and a catalyst-loaded RDE as a working electrode. The Ag/AgCl electrode was calibrated to an RHE based on our reported method.[S1] Before electrochemical measurements, working electrodes were electrochemically cleaned by repeated potential cycles between 1.0 and 1.4 V vs. RHE with a scan rate of 50 mV s^{-1} until their cyclic voltammograms became stable. The OER polarization curves of catalysts were obtained by LSV measurements in O_2-saturated 0.5 M H_2SO_4 at a scan rate of 5 mV s^{-1} with a rotating speed of 1600 rpm. The potential drop due to the ohmic resistance (*iR*) was corrected. OER polarization curves were fitted to the Tafel equation ($\eta = a + b \log j$, where η, *a*, *b*, and *j* are the overpotential, exchange current density, Tafel slope, and current density, respectively) to obtain the Tafel slopes. To estimate the ECSAs of catalysts, a working electrode was held at 0.1 V vs. RHE in CO-saturated 0.5 M H_2SO_4. Then, the monolayer of adsorbed CO was oxidized and removed by a potential sweep from 0.3 to 1.4 V vs. RHE at a scan rate of 20 mV s^{-1} in 0.5 M H_2SO_4, which was purged with Ar before use. Based on the charge estimated from the area under the CO oxidation peak, which was integrated after background subtraction,[S2] and the charge required for the oxidation of a monolayer of CO, 358 μC cm^{-2},[S3] the ECSAs of catalysts were calculated.

References

(S1) Y. Kim, Y. W. Lee, S. Lee, J. Gong, H.-S. Lee and S. W. Han, *ACS Appl. Mater. Interfaces*, 2021, **13**, 45538–45546.

(S2) F. Bizzotto, J. Quinson, A. Zana, J. Kirkensgaard, A. Dworzak, M. Oezaslan and M. Arenz, *Catal. Sci. Technol.*, 2019, **9**, 6345–6356.

(S3) S. Alia, K. Hurst, S. Kocha and B. Pivovar, *J. Electrochem. Soc.*, 2016, **163**, 3051–3056.

2. Supplementary figures

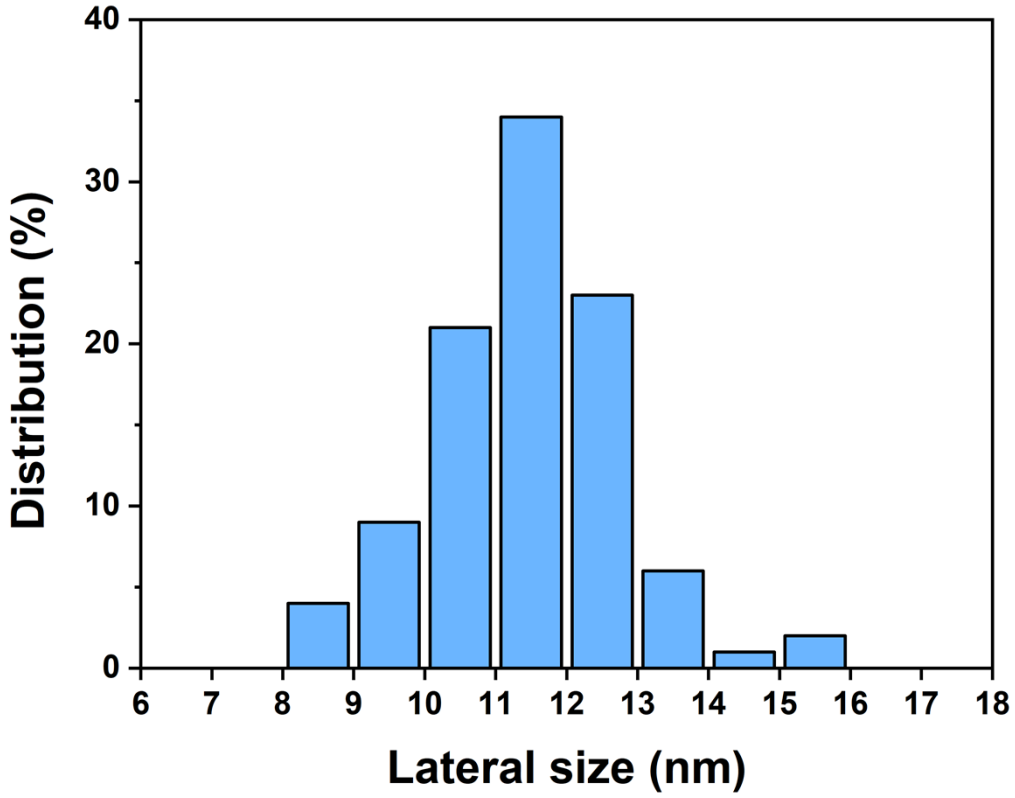

Fig. S1 TEM-determined lateral size distribution of Ir nanosheets. The average lateral size of the prepared Ir nanosheets was 11.5 ± 1.3 nm, which was estimated from more than 100 nanosheets. For each nanosheet, the longest lateral length was taken as its lateral size.

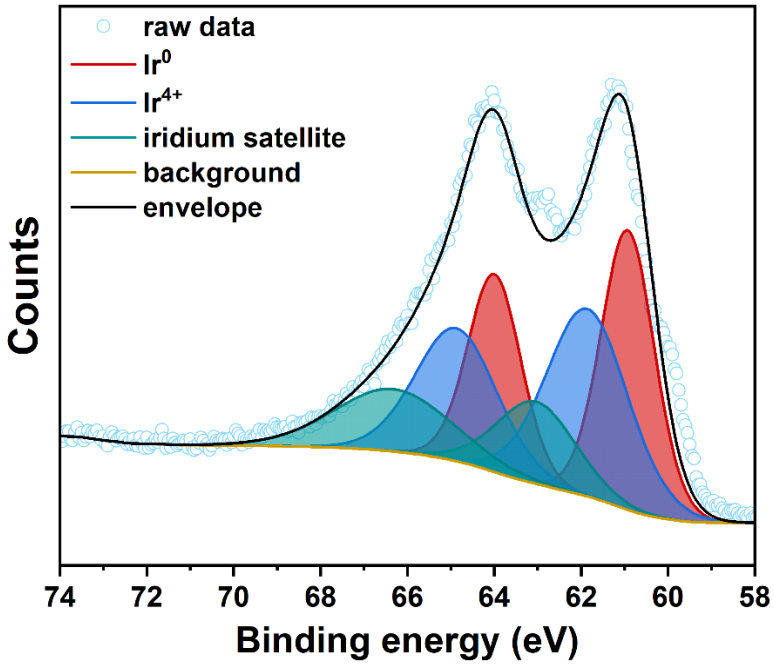

Fig. S2 Ir 4f core-level XPS spectrum of a commercial Ir black, showing metallic Ir $4f_{5/2}$ and $4f_{7/2}$ peaks at binding energies of 64.0 and 60.9 eV, respectively, and Ir(IV) peaks at 61.9 and 64.9 eV. The areas under the metallic Ir and Ir(IV) peaks are almost the same.

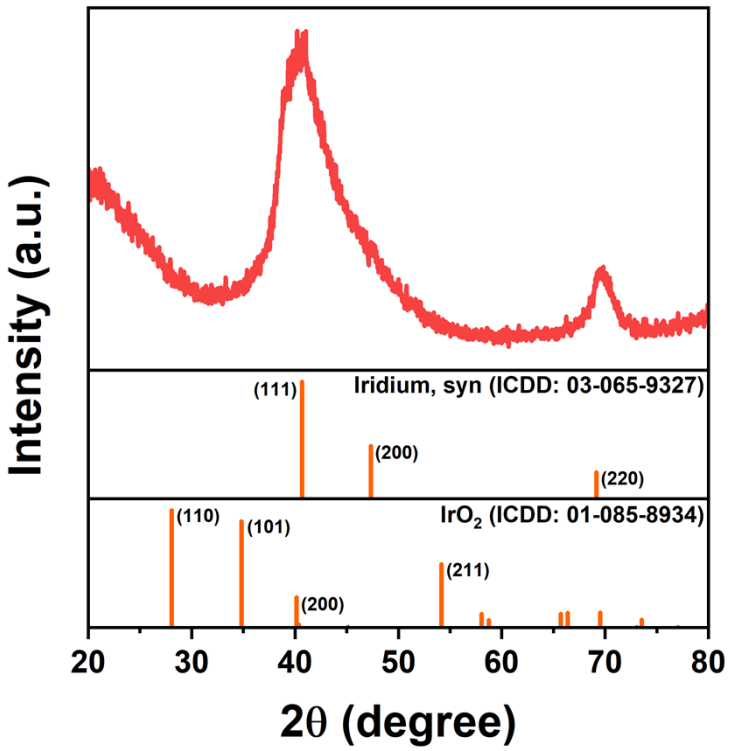

Fig. S3 XRD pattern of Ir nanosheets, indicating the fcc metallic structure of the prepared Ir nanosheets. The (200) diffraction peak of the Ir nanosheets cannot be clearly discerned because of the peak broadening originating from the small crystallite size of the Ir nanosheets. The peak positions and relative intensities of the Ir and IrO_2 references were taken from the ICDD database.

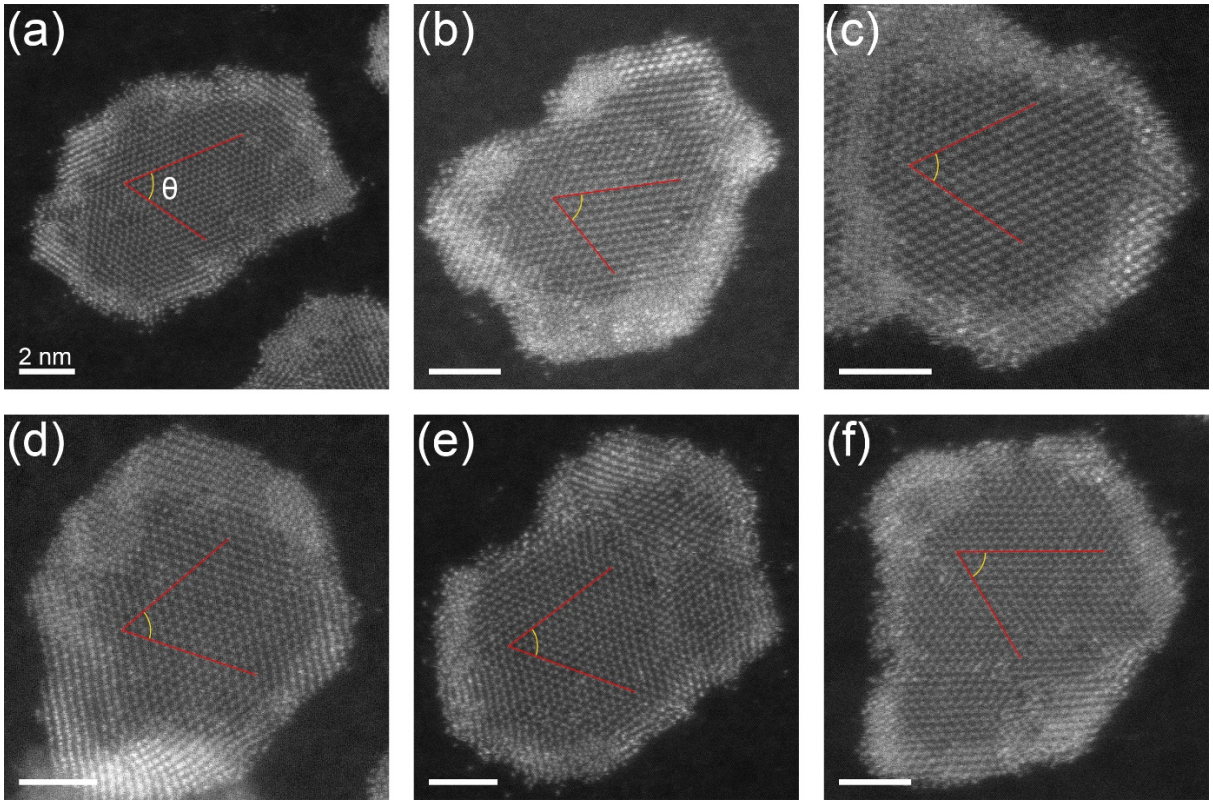

Fig. S4 HAADF–STEM images of Ir nanosheets. Scale bars indicate 2 nm. Part a was reproduced from Fig. 1c. The angles between the crystal lattice axes (θ) were (a) 57.72°, (b) 58.98°, (c) 60.53°, (d) 58.87°, (e) 57.14°, and (f) 57.37°. Based on these values, the average angle of the distortion (|Δθ|) from the ideal lattice could be estimated to be 1.65 ± 1.24°.

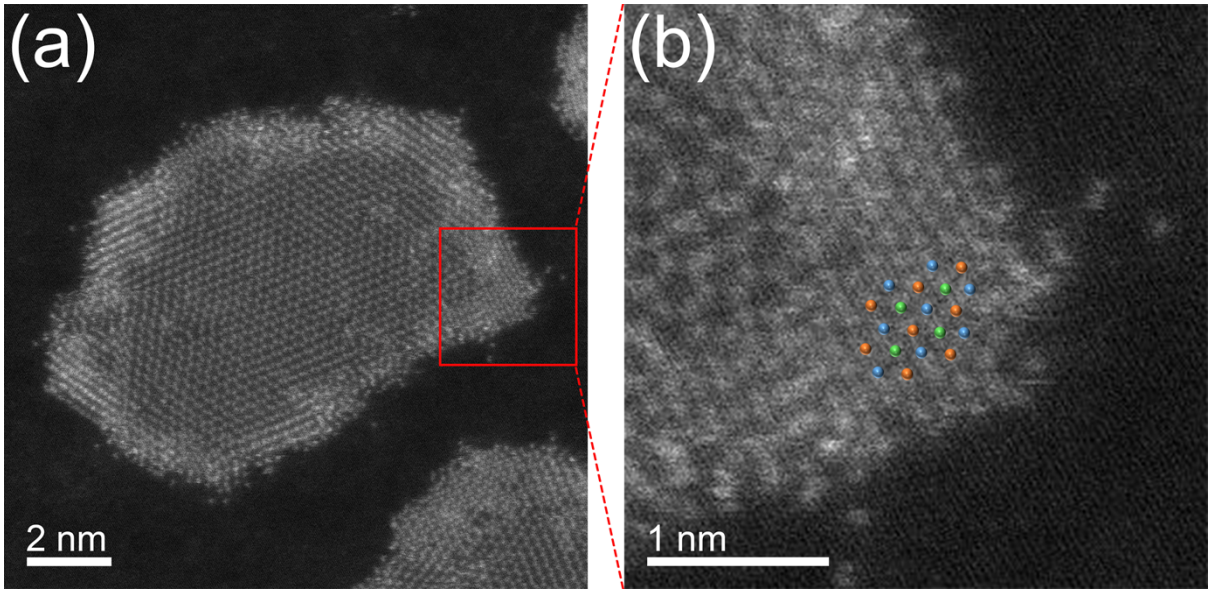

Fig. S5 (a) HAADF–STEM image of an Ir nanosheet. (b) Magnified HAADF–STEM image of the red square region in part a. The typical atomic arrangement of a fcc structure with three atomic layers is included, in which atoms in each layer are denoted with different colors.

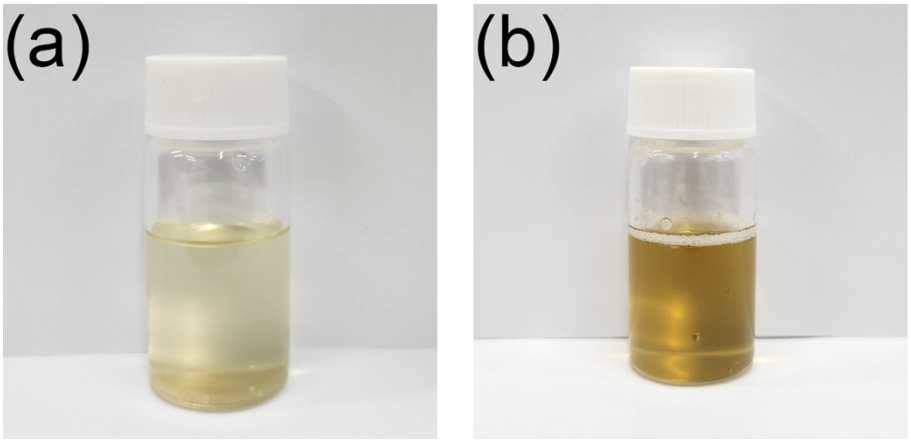

Fig. S6 Photographs of the reaction solution containing Ir precursors and di-*n*-octylamine solvent (a) before and (b) after the addition of *n*-butyllithium.

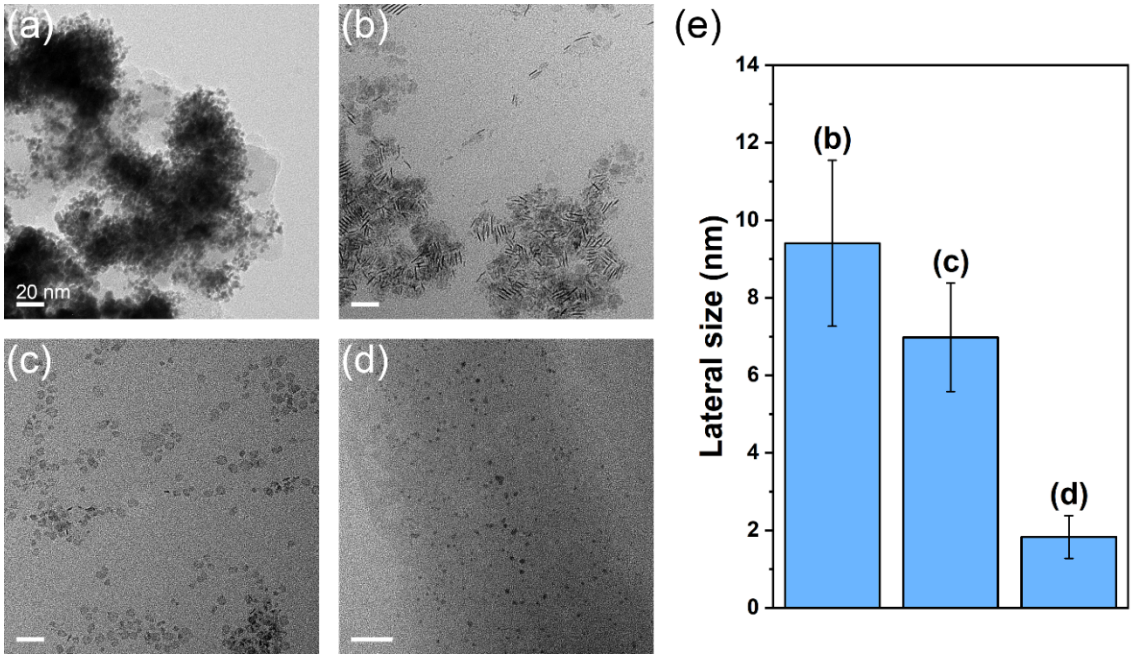

Fig. S7 (a) TEM image of nanostructures prepared in the absence of *n*-butyllithium under otherwise synthesis conditions identical to those employed for the typical preparation of Ir nanosheets. TEM images of nanostructures prepared by injecting *n*-butyllithium into the reaction solution (b) right after starting the CO flow, (c) after the reaction temperature reached 160 °C, and (d) after the reaction temperature reached 290 °C. Scale bars indicate 20 nm. (e) The average lateral sizes of nanostructures estimated from the TEM images shown in parts b–d. The sizes of more than 50 nanostructures were measured for each sample.

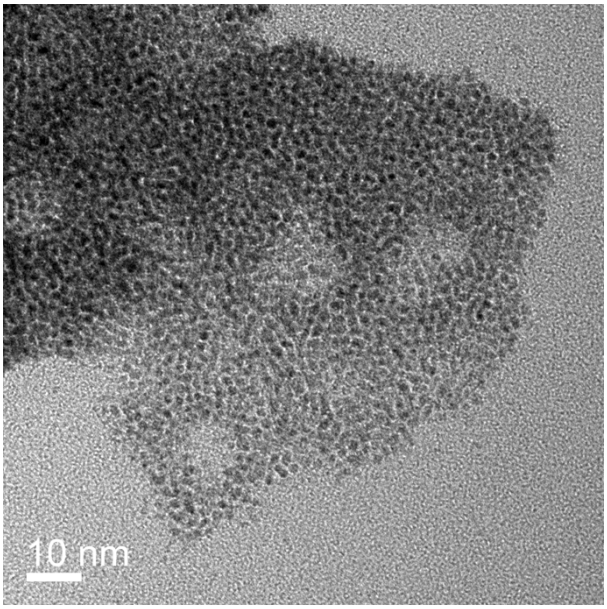

Fig. S8 TEM image of nanostructures prepared in the absence of CO under otherwise synthesis conditions identical to those employed for the typical preparation of Ir nanosheets.

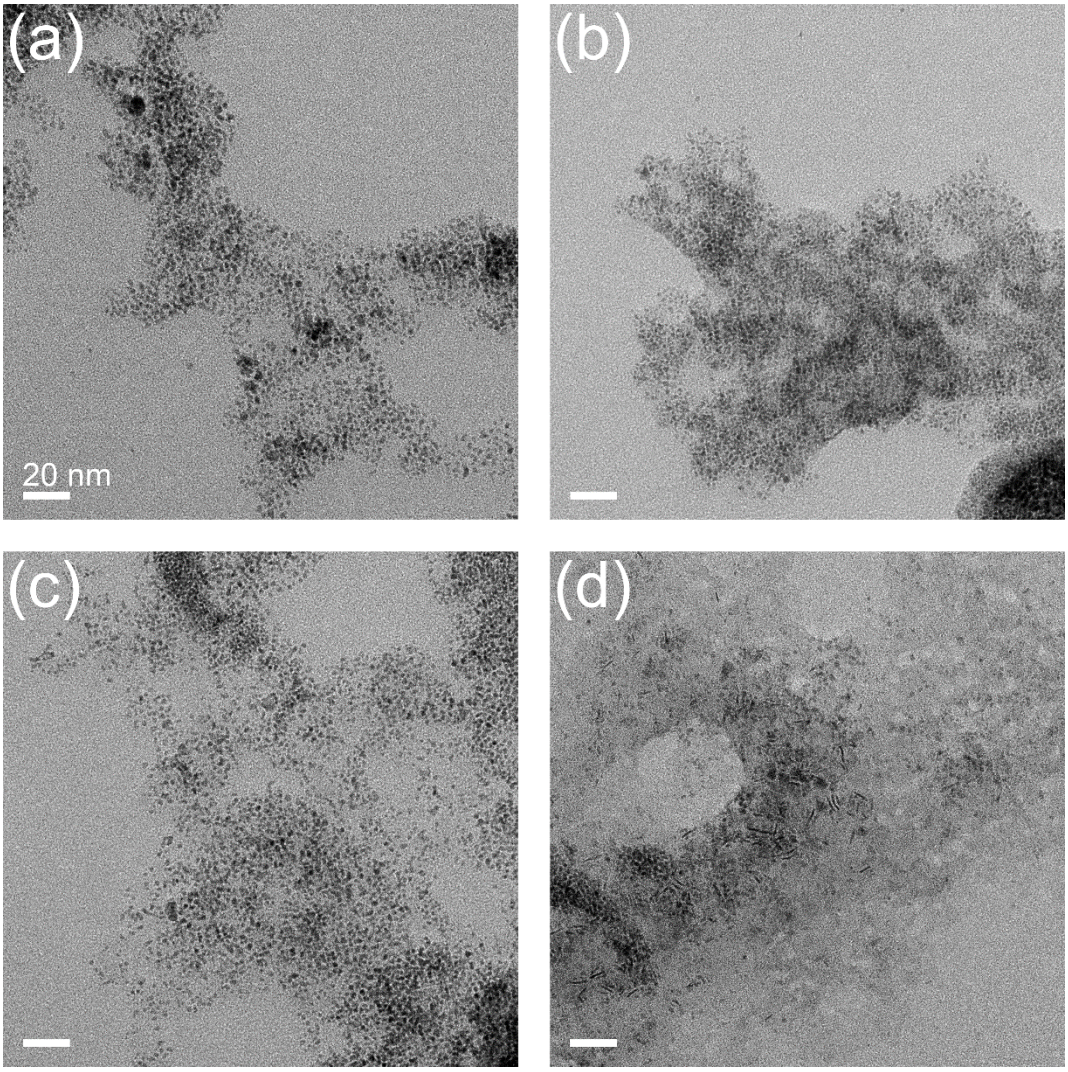

Fig. S9 TEM images of nanostructures prepared at reaction temperatures different from that of the standard synthesis (290 °C): (a) 210, (b) 230, (c) 250, and (d) 270 °C. Other synthesis conditions were identical to those employed for the typical preparation of Ir nanosheets.

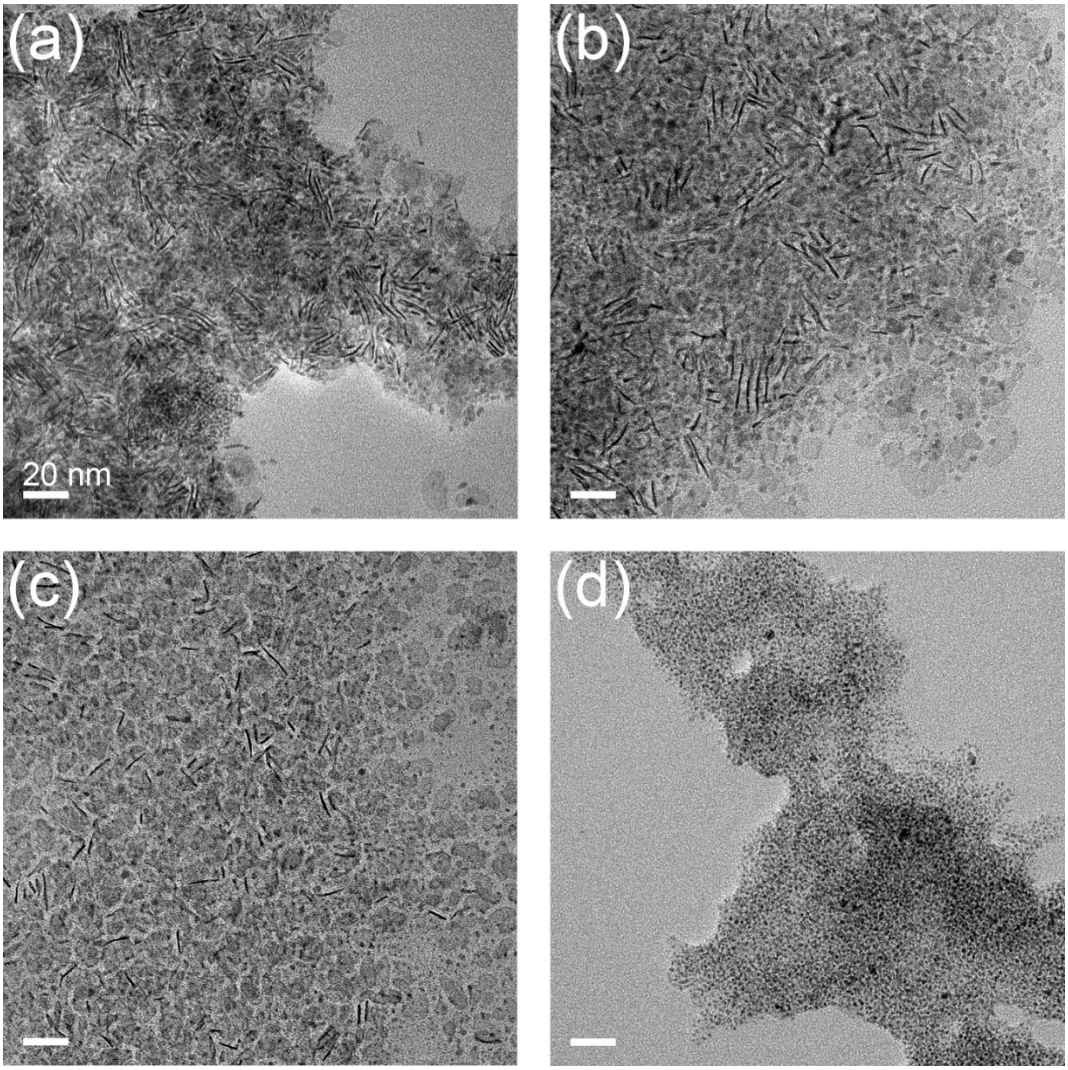

Fig. S10 TEM images of nanostructures prepared with (a) $IrBr_4$, (b) IrI_4, (c) oleylamine, and (d) trioctylamine under otherwise synthesis conditions identical to those employed for the typical preparation of Ir nanosheets. Scale bars indicate 20 nm. 0.0512 g of $IrBr_4$ and 0.0700 g of IrI_4 were used instead of $IrCl_4$, and 10 mL of oleylamine and trioctylamine solvents were used instead of di-*n*-octylamine in the control experiments.

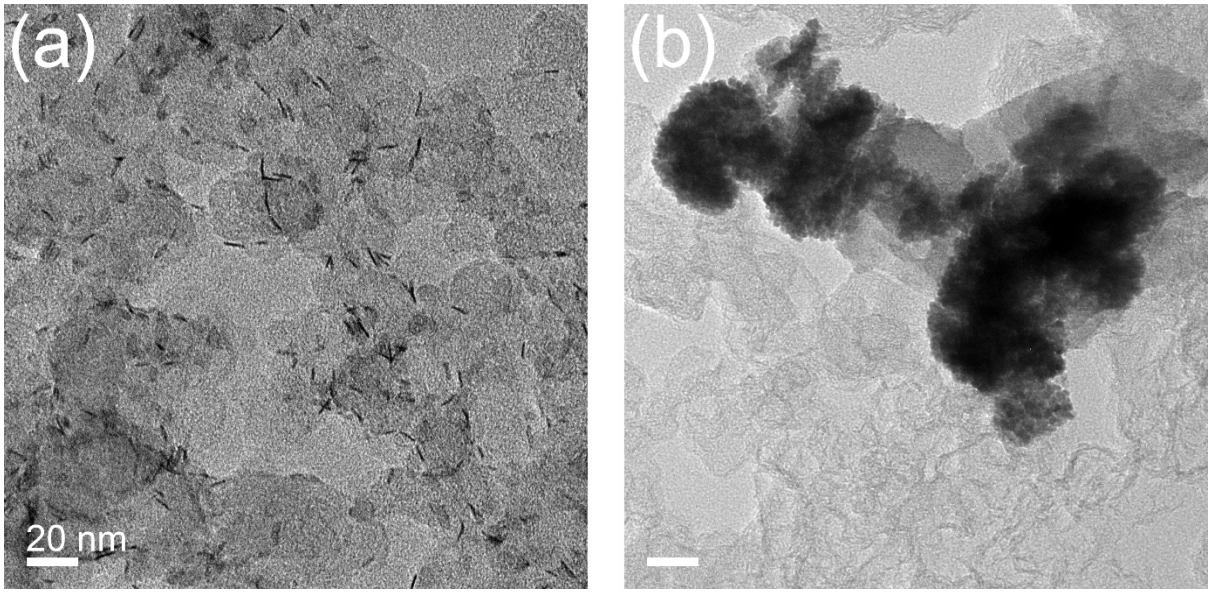

Fig. S11 TEM images of (a) Ir nanosheets and (b) Ir black particles (average size = 34.6 ± 4.1 nm) supported on a carbon black support (Vulcan XC-72R).

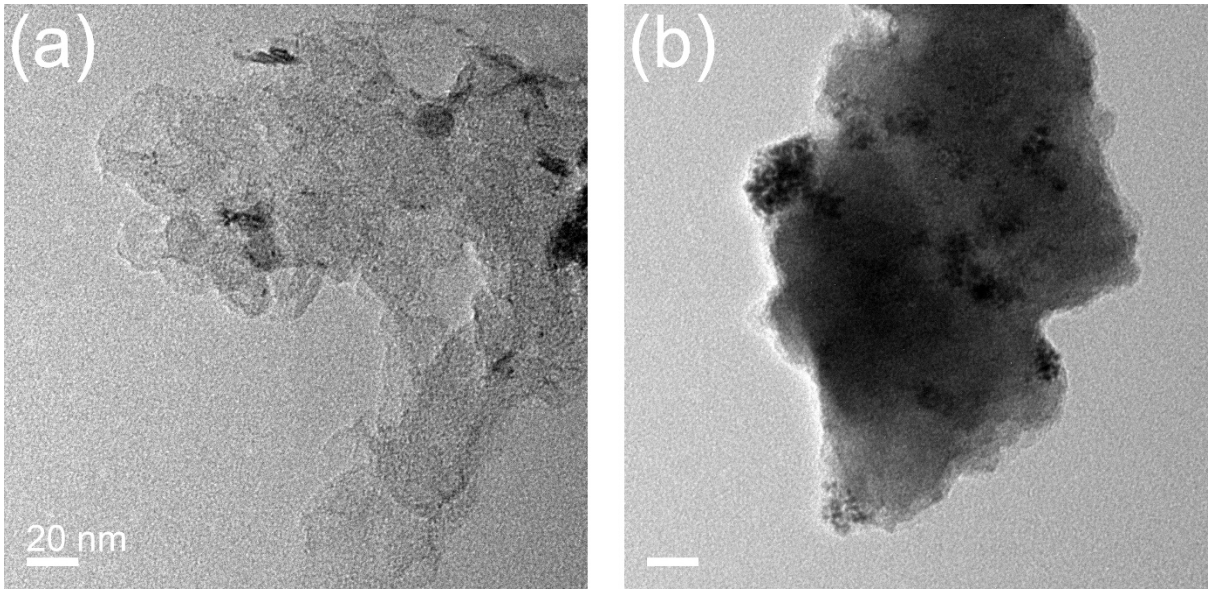

Fig. S12 TEM images of (a) Ir nanosheet and (b) Ir black catalysts after the long-term durability test.

Table S1 OER properties of various Ir-based catalysts in acidic media.

Catalysts	Electrolyte	η@10 mA cm^{-2} (mV)	Tafel slope (mV dec^{-1})	Mass activity* (A g_{Ir}^{-1})	Reference
ultrathin Ir nanosheets	0.5 M H_2SO_4	272.2	54.5	476.8[a]	this work
Ir nanoparticles on graphite foam	0.5 M H_2SO_4	290	46	200[b]	33
IrO_x–Ir	0.5 M H_2SO_4	295	43.7–44.7	8[c]	34
IrO_2 on carbon nanotube	0.5 M H_2SO_4	293	32	-	35
amorphous Ir nanosheets	0.1 M $HClO_4$	255	40	221.8[a]	21
partially hydroxylated Ir nanosheets	0.5 M H_2SO_4	328	45.4	209[a]	23
IrCuNi concave nanocube	0.1 M $HClO_4$	273	41	6600[a]	36
$IrHfO_x$	0.1 M $HClO_4$	300	60	6950[a]	37
$Ir_{44}Pd_{10}$ nanocube	0.1 M $HClO_4$	226	53.9	1990[c]	38
PdCu/Ir core/shell nanocrystal	0.1 M $HClO_4$	283	59.6	1830[d]	39
Ir layer on Pd nanocrystal	0.1 M $HClO_4$	300	84.9	1010[a]	40

*Mass activities were measured at 1.53,[a] 1.62,[b] 1.48,[c] and 1.51 V[d] vs. RHE.